Modeling of Trade Wind Cumuli with a Low-Order Turbulence Model: Toward a Unified Description of Cu and Sc Clouds in Meteorological Models

P. BECHTOLD, J. W. M. CUIJPERS,* P. MASCART, AND P. TROUILHET

Laboratoire d'Aérologie, Université Paul Sabatier, Toulouse, France

(Manuscript received 3 December 1993, in final form 28 June 1994)

ABSTRACT

A simple method is proposed to extend a low-order turbulence scheme including a subgrid-scale cloudiness scheme to represent not only nonconvective (stratiform) cloudiness and turbulence but also shallow, nonprecipitating cumulus convection by utilizing an appropriate subgrid-scale distribution function. A simple approach is chosen that avoids the knowledge of the skewness parameter. All cloud water–related variables (cloud water content, partial cloudiness, liquid water flux) are computed by interpolating linearly as a function of the saturation deficit between two limit cases: the stratocumulus case, which can be well represented by a Gaussian distribution function, and the trade wind cumulus case, characterized by a positively skewed distribution function with a skewness of 2.

Comparisons of the scheme with a third-order turbulence scheme and large-eddy simulations (LES) for the Puerto Rico Field Experiment show satisfying results. It is shown that the liquid water flux term, which is strongly dependent on the distribution chosen, is the crucial parameter of the scheme.

1. Introduction

Currently, there exist essentially three types of models to represent the trade wind boundary layer, which is characterized by small scattered cumulus clouds. The first type includes 3D large-eddy simulation (LES) models (e.g., Sommeria 1976; Schumann and Moeng 1991; Cuijpers and Duynkerke 1993, hereafter CD93), which resolve the cumulus updrafts explicitly, and 2D cumulus ensemble models (Krueger 1988; Krueger and Bergeron 1994) covering a mesoscale domain. Under the second type we can regroup 1D higher (third)-order turbulence models (Bougeault 1981a,b; hereafter B81a,b), which make use of a subgrid-scale cloudiness scheme. Finally, the third group includes mixed-layer models (Betts 1973; Albrecht et al. 1979) and bulk models (Randall et al. 1992), where the boundary layer is represented by a small number of layers (typically one to three) and where the turbulent flux in the boundary layer is computed from the surface flux and the entrainment rate only.

The common part of all these models (maybe to a smaller degree for the more specialized mixed-layer models) is that they can also be successfully used to simulate the stratocumulus-capped boundary layer. However, in mesoscale numerical weather prediction models (Ballard et al. 1991; Pudykiewicz et al. 1992) and GCMs (Tiedtke 1989), the trade wind boundary layer is generally parameterized with the aid of a shallow convection scheme (based on a cloud model), whereas the turbulence mixing scheme is only used to describe nonconvective (stratiform) cloudiness. Of course, the use of a shallow convection scheme and a turbulence scheme to describe the mean turbulent transport in the boundary layer is somewhat artificial, and it might be desirable to use only one unified cloudiness–turbulence scheme. The advantage of such a scheme is that it also correctly represents the momentum flux and allows for a detailed treatment of microphysics (precipitation) in partly cloudy layers (Bechtold et al. 1993). The application of such a scheme is especially useful for mesoscale models, where increasing computer power allows for the use of a high-resolution ($\Delta z \approx 100$ m) turbulence scheme based on a prognostic equation for the turbulent kinetic energy.

Recently, Bechtold et al. (1992, hereafter BFP92) applied a numerically efficient 1.5-order turbulence scheme coupled with a subgrid-scale cloudiness scheme based on a Gaussian (nonskewed) probability distribution for the conservative thermodynamic variables to various cloud-topped boundary layer cases [decoupled Sc boundary layer, Sc–Cu cloudiness transition]. Their results indicated that this type of modeling (belonging to the second type of the above classification) can reproduce observed cloud amounts of, say, larger than 20% reasonably well. However, for

* On leave: IMAU/RUU, Utrecht, the Netherlands.

Corresponding author address: Dr. Peter Bechtold, Laboratoire d'Aérologie, URA 354, Université Paul Sabatier, 118 Route de Narbonne, Toulouse, cedex 31062, France.

lower cloud amounts the Gaussian assumption fails to reproduce the observed boundary layer structure.

In LES models the subgrid-scale distribution of the conservative variables can be assumed Gaussian, whereas the subgrid-scale distribution in ensemble-mean turbulence schemes, which are representative of larger areas, depends on the situation (Cu or Sc boundary layer). In particular, one observes that the skewness of the subgrid distribution increases with decreasing cloudiness (Bougeault 1982; Randall 1987). Bougeault (1982) suggested a Gamma function with variable skewness as the simplest general distribution function. Recently, Lewellen and Yoh (1993) proposed a new formulation of partial cloudiness based on the combination of two multivariate normal distributions. However, both the formulation of Bougeault and that of Lewellen and Yoh require the skewness as input, an unknown parameter in low-order turbulence schemes.

The aim of this paper is to show that an order 1.5 turbulence model can also be extended to the trade wind (low cloudiness) boundary layer when we linearly interpolate between the Gaussian distribution and a distribution with known constant positive skewness. In the following, we show how the cloudiness scheme is coupled to the turbulence scheme and lay out the importance of the buoyancy flux term formulation in the turbulent kinetic energy equation. Finally, the ability of the generalized cloudiness–turbulence scheme is illustrated with a 1D simulation of the Puerto Rico Experiment (Pennell and LeMone 1974), already modeled by Sommeria (1976), B81b, and CD93.

2. Subgrid-scale cloudiness

Before discussing the turbulent buoyancy flux in partly cloudy layers, we first briefly recall some features of the statistical partial cloudiness scheme [see Mellor (1977), B81a, and Chen (1991) for further discussion]. The scheme is based on the prognostic quasi-conservative variables liquid potential temperature

$$\theta_l = \theta(1 - Lq_l/c_pT) \tag{1}$$

and total water content

$$q_w = q_v + q_l. \tag{2}$$

All notations are conventional. Ensemble-mean values will be denoted by overbars, and primes will denote deviations from the ensemble mean. We desire expressions for the partial cloudiness N and the ensemble-mean cloud water content $\bar{q}_l$. The local liquid water content is given by $q_l = \max[(q_w - q_s), 0]$, where q_s is the saturation specific humidity. Defining the continuous variable $s = q_w - q_s$ and using a truncated Taylor expansion for q_s,

$$\begin{aligned} q_s(T) &= \bar{q}_{sl} + \bar{q}_{sl,T}(T - \bar{T}_l) \\ &= \bar{q}_{sl} + \bar{q}_{sl,T}(\theta_l'\bar{T}/\bar{\theta} + Lq_l/c_p], \end{aligned} \tag{3}$$

with

$$\bar{q}_{sl} = q_s(\bar{T}_l),\ \bar{q}_{sl,T} = (\partial q_s/\partial T)_{T=\bar{T}_l},\quad \bar{T}_l = \bar{\theta}_l(\bar{T}/\bar{\theta}), \tag{4}$$

we can entirely express s in terms of fluctuations of the conservative variables:

$$s = aq_w' - b\theta_l' + c, \tag{5}$$

where

$$a = (1 + L\bar{q}_{sl,T}/c_p)^{-1},\quad b = a(\bar{T}/\bar{\theta})\bar{q}_{sl,T},\quad c = a(\bar{q}_w - \bar{q}_{sl}). \tag{6}$$

We can now compute the partial cloudiness and the ensemble-mean liquid water content given a distribution function G for the normalized variable $t = s/\sigma_s$, where $\sigma_s = (\overline{s'^2})^{1/2}$:

$$N = \int_0^{+\infty} G(t)dt \tag{7}$$

$$\bar{q}_l/\sigma_s = \int_0^{+\infty} tG(t)dt. \tag{8}$$

In order to couple the cloudiness scheme to the turbulence scheme we further need the expression for the covariance $\overline{sq_l'}$:

$$\overline{sq_l'}/\sigma_s^2 = \int_0^{+\infty} (t - Q_1)tG(t)dt. \tag{9}$$

The partial cloudiness and the normalized liquid water content are functions of the normalized saturation deficit $Q_1 = c/\sigma_s$ only. In order-1.5 turbulence schemes, the standard deviation σ_s must be parameterized. One possible parameterization based on the stationary equations for the second-order moments has been derived in BFP92, where it has further been assumed that the mean-gradient production term exactly balances the dissipation term

$$\sigma_s = (c_1 l_K l_\epsilon)^{1/2}\left[a^2\left(\frac{\partial \bar{q}_w}{\partial z}\right)^2 + b^2\left(\frac{\partial \bar{\theta}_l}{\partial z}\right)^2 - 2ab\frac{\partial \bar{q}_w}{\partial z}\frac{\partial \bar{\theta}_l}{\partial z}\right]^{1/2}, \tag{10}$$

where l_K and l_ϵ stand for the turbulent mixing and dissipation length scales, and where c_1 is a constant of value 0.32.

3. Buoyancy flux in partly cloudy layers

a. General formulation

The buoyancy flux term is the main production term of turbulent kinetic energy in the cloud layer. Using the virtual potential temperature

$$\begin{aligned} \theta_v &= \theta(1 + 0.61q_w - 1.61q_l) \\ &= \theta_l + \alpha q_w + \beta q_l \end{aligned} \tag{11}$$

with

$$\alpha = \theta 0.61, \quad \beta = \frac{\theta}{T}\frac{L}{c_p} - 1.61\theta, \tag{12}$$

the buoyancy flux becomes

$$\overline{w'\theta_v'} = (1 + 0.61\bar{q}_w)\overline{w'\theta_l'} + \alpha\overline{w'q_w'} + \beta\overline{w'q_l'}. \tag{13}$$

In (13) and the following the coefficients α and β should be read as $\alpha = \bar{\alpha}$ and $\beta = \bar{\beta}$. Note that the coefficient β is about one magnitude larger than α. In order to determine the buoyancy flux, the liquid water flux in (13) must also be expressed as a function of the fluxes of the conservative variables. Dimensional arguments lead to the following expression for the liquid water flux:

$$\overline{w'q_l'} = \gamma\overline{w's}\frac{\overline{sq_l'}}{\sigma_s^2} = \gamma[a\overline{w'q_w'} - b\overline{w'\theta_l'}]\frac{\overline{sq_l'}}{\sigma_s^2}, \tag{14}$$

where γ is a proportionality coefficient. The coefficients a and b are given in (6), and $\overline{sq_l'}/\sigma_s^2$ is obtained from (9). As shown by Chen (1991), for $\gamma = 1$ (14) is exactly verified in the Gaussian limit. Preliminary studies using LES indicate that γ increases with decreasing Q_1 with values ranging between 1 and 5. For simplicity, a constant value of 1 is applied here. Then the buoyancy flux can be written as

$$\overline{w'\theta_v'} = \overline{w'\theta_l'}\left[1 + 0.61\bar{q}_w - \beta b\frac{\overline{sq_l'}}{\sigma_s^2}\right] + \overline{w'q_w'}\left[\alpha + \beta a\frac{\overline{sq_l'}}{\sigma_s^2}\right]. \tag{15}$$

Inside the cloud layer $\overline{w'\theta_l'}$ is negative, but $\overline{w'q_w'}$ is positive, so that the two terms in (15) related to the liquid water flux are always buoyancy production terms. In the case of a Gaussian distribution $\overline{sq_l'}/\sigma_s^2$ is equal to the partial cloudiness N. However, it becomes a strongly nonlinear function of $N(Q_1)$ when other distribution functions are used; for example, if a positively skewed distribution is chosen with a skewness factor of 2, $\overline{sq_l'}/\sigma_s^2$ becomes (see appendix A) $(2 - Q_1)e^{Q_1 - 1} = (1 - \ln N)N \approx 4N$ for $N = 5\%$.

b. Relation to convection schemes

In convection schemes, the turbulent diffusion term in the prognostic equations for the conservative thermodynamic variables is expressed as a convective transport term computed with the aid of a cloud model. In order 1.5 turbulence schemes, the turbulent diffusion terms are expressed as a function of the turbulent kinetic energy, which in convective situations is mainly produced by the buoyancy flux term (15). It is therefore the formulation of the buoyancy flux that links the two concepts. Denoting the buoyancy flux as

$$F_{\theta_v} = AF_{\theta_l} + BF_{q_w}, \tag{16}$$

with $F_{\theta_v} = \overline{w'\theta_v'}$, $F_{\theta_l} = \overline{w'\theta_l'}$, $F_{q_w} = \overline{w'q_w'}$, and A and B as two coefficients having different values for the totally saturated (cloudy) and unsaturated (clear sky) buoyancy flux (see CD93), we can derive an expression for the buoyancy flux in partly cloudy layers as a sum of the saturated and unsaturated fluxes. Assuming that $\overline{sq_l'}/\sigma_s^2 = N(1 + f_{\mathrm{NG}})$, where f_{NG} is the non-Gaussian contribution to the flux, (15) can be rewritten as (see appendix B for a detailed derivation)

$$F_{\theta_v} = NF_{\theta_v}^{\mathrm{cld}} + (1 - N)F_{\theta_v}^{\mathrm{clr}} + \beta N f_{\mathrm{NG}}(aF_{q_w} - bF_{\theta_l}). \tag{17}$$

Here the superscripts cld and clr denote the cloudy and clear sky fluxes as defined by (16) (see also appendix B). The first two terms of the rhs of (17) are identical to the Gaussian flux relation derived by Sommeria and Deardorff (1977); the additional third term appears due to the non-Gaussian part of the flux.

Using a convective mass flux scheme (the boundary layer is partitioned into updraft and downdraft areas) Randall (1987) derived the following expression for the buoyancy flux in partly cloudy layers:

$$F_{\theta_v} = (1 - \tilde{N})F_{\theta_v}^{\mathrm{cld}} + \tilde{N}F_{\theta_v}^{\mathrm{clr}} - \omega_*/g[1 - 1.61c_pT/L]L\tilde{q}_l, \tag{18}$$

where g is the gravity constant, $\omega_* = \tilde{N}(1 - \tilde{N})(w^u - w^d)$ is the convective mass flux (superscripts u and d denote properties of the updrafts and downdrafts, respectively), and $\tilde{q}_l$ is a measure of the relative humidity of the mean flow. As in (17) we can identify three terms in (18). However, comparing (17) and (18) we see that the weighting factors for the first two rhs terms are just reversed. Nevertheless, $\tilde{N}$ denotes strictly speaking the fractional updraft region, which is a function of the vertical velocity skewness only (Randall et al. 1992). Here $\tilde{N}$ is always smaller than N; for example, in the Sc case $\tilde{N}$ is about 0.5, while $N = 1$.

For the reasons given above it is difficult to make an exact analogy between the buoyancy flux in partly cloudy layers derived from a turbulence scheme (statistical cloud scheme) and a mass flux scheme. However, one can qualitatively identify in each scheme the three different flux contributions. A promising partial cloudiness parameterization that provides a smooth transition between the Gaussian statistical model and the updraft and downdraft model was recently proposed by Lewellen and Yoh (1993). The partial cloudiness and the mean liquid water content are parameterized as the sum of two Gaussian probability distribution functions (pdf), depending on the skewness of s, whereas the liquid water content involves also the parameters determining the vertical velocity pdf. Unfortunately, the method proposed by Lewellen and Yoh is not yet accessible to low-order turbulence schemes typically used in mesoscale and large-scale models, as it involves too many unknown parameters.

c. *Choice of the distribution*

Motivated by the linear model of Lewellen and Yoh and trying to keep the number of free parameters of the cloudiness scheme as small as possible, we decided to compute the cloud water–related variables from (7)–(9) by a linear interpolation between two limit distributions, one for the Sc case and one for the trade wind cumulus case. The form of the distributions as well as the interpolation parameter still have to be determined.

The discussion of the choice of the distribution function will be made with the aid of three diagrams (Figs. 1a,b,c) taken from Bougeault (1982). The diagrams show the partial cloudiness, the ensemble-mean cloud water content, and $\overline{sq_l'}/\sigma_s^2$ as a function of the normalized saturation measure Q_1 for different values of the skewness, $\overline{s^3}/(\overline{s^2})^{3/2}$. The values were computed using a gamma function with variable skewness. We will especially concentrate on the curves obtained with a skewness (hereafter skewness is referred to as the skewness of s) between 0 and 2, respectively. We see that for $Q_1 > -1$ the values of the partial cloudiness and the mean liquid water content only weakly depend on the value of the skewness (the choice of the distribution function), whereas the $\overline{sq_l'}/\sigma_s^2$ flux is nearly independent of the value of the skewness (large negative values excluded) for $Q_1 > 0$ but strongly depends on the value of the skewness for lower values of Q_1. This is a very important result because it says that for values of $Q_1 > 0$ (corresponding to values of the partial cloudiness of 20%–50% and more) the results are not sensitive to the choice of the distribution function, a result that has also been confirmed by Lewellen and Yoh (see their Figs. 2–5). This means that the stratocumulus-topped boundary layer can be reasonably well simulated with any distribution function. Typical maximum values of the skewness in the trade wind boundary layer range between 2 and 3 (Cuijpers 1994). Here we retained the value of 2, as for this value a simple analytical distribution function can be constructed (B81).

Given the above results we decided to interpolate linearly as a function of Q_1 between the two extreme cases, the stratocumulus case [using a Gaussian function in (7)–(9)] and the trade wind case (using an exponential function proposed by B81a with a constant skewness factor of 2). So we finally get

$$\Psi = \begin{cases} \Psi_{\text{Gauss}}, & Q_1 > 0 \\ 0.5[-Q_1\Psi_{\text{exp}} + (2 + Q_1)\Psi_{\text{Gauss}}], & -2 \leq Q_1 \leq 0 \\ \Psi_{\text{exp}}, & Q_1 < -2, \end{cases} \tag{19}$$

where Ψ stands for either of the variables N or $\bar{q}_l$. The expressions for these variables obtained with a Gaussian (subscript Gauss) and an exponential function (subscript exp) are listed in the appendix A. However, for the interpolation of the $\overline{sq_l'}/\sigma_s^2$ covariance, which is

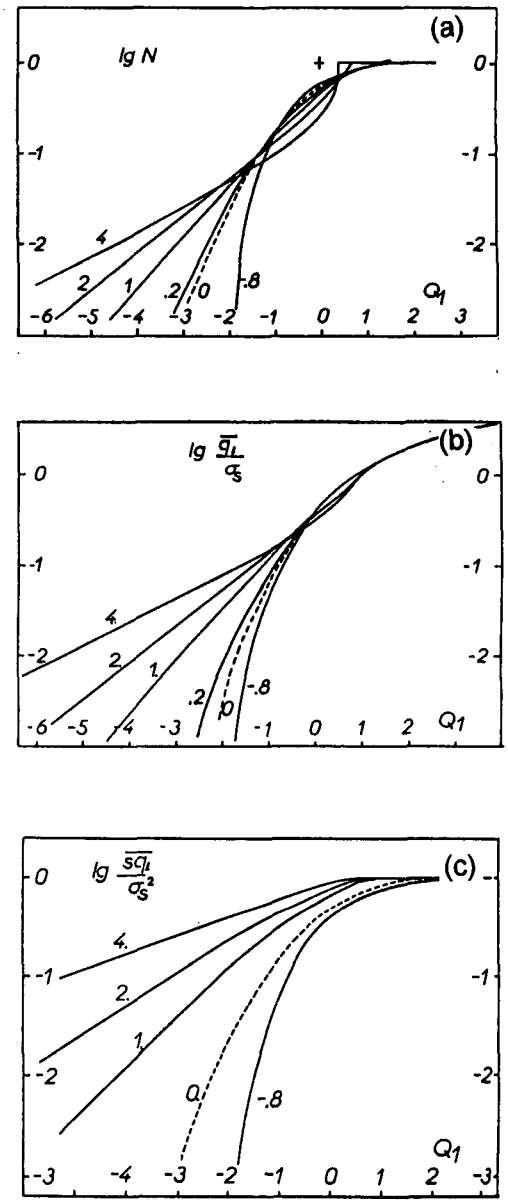

FIG. 1. Parameterized partial cloudiness (a), mean cloud water content (b), and $\overline{sq_l'}/\sigma_s^2$ (c) as a function of Q_1 for a gamma function with different values of the skewness parameter (after Bougeault 1982).

(as will be shown later) the most critical parameter of the scheme, we adopted a slightly different formulation. It can be shown that $\overline{sq_l'}/\sigma_s^2$ can be expressed as the product of the partial cloudiness N multiplied by a nondimensional factor $F_{\text{NG}} = (1 + f_{\text{NG}})$, which we will call here the non-Gaussian transport factor. Only in the case of a Gaussian distribution does this factor have the constant value of one; otherwise it is a function of Q_1. In Fig. 2 we have plotted the value of F_{NG} as a function of Q_1 for the two chosen limit distribution models. The interpolation of the $\overline{sq_l'}/\sigma_s^2$ covariance between the two limit distributions is done by interpolating linearly the F_{NG}

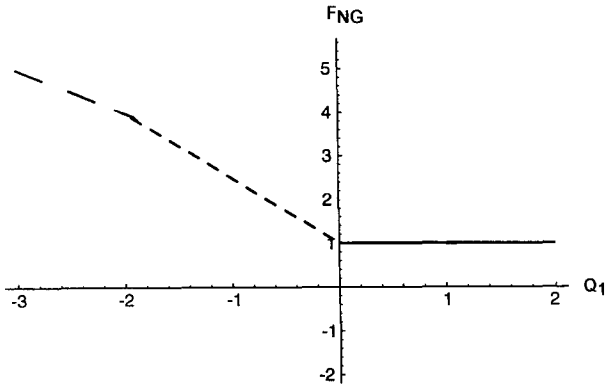

FIG. 2. Nonlinear transport factor F_{NG} for different distributions as a function of Q_1. Gaussian distribution: solid line, exponential distribution (skewness 2): long-dashed line, and present model: short-dashed line.

(dashed line in Fig. 2) and multiplying by N, already obtained from (19). Thus, using Fig. 2, we obtain

$$\overline{sq_l}/\sigma_s^2 = NF_{NG}$$

$$F_{NG} = \begin{cases} 1, & Q_1 > 0 \\ 1-1.5Q_1, & -2 \leq Q_1 \leq 0 \\ 2-Q_1, & Q_1 < -2. \end{cases} \quad (20)$$

Furthermore, we impose a Gaussian liquid water flux at the top and the base of the cloud layer, where the skewness of s tends to zero (Bougeault 1982).

4. Puerto Rico case

a. Model intercomparison

The cloudiness scheme described above has been included in a 1D version of the mesoscale model described in BFP92. The fair weather trade wind boundary layer observed during the Puerto Rico Experiment (Pennell and LeMone 1974) has been chosen to validate the model. Numerous previous numerical studies of this experiment are available for comparison, and here we will make extensive use of the LES simulations of Sommeria (1976, hereafter S76) and CD93, as well as of the 1D simulations done with a third-order turbulence scheme by B81b.

The model was initialized following B81b; that is, we imposed a large-scale divergence of 7×10^{-6} s^{-1} and a radiative flux divergence of 3×10^{-5} K s^{-1}. The turbulent kinetic energy was initialized by a linear profile throughout the boundary layer. The initial profiles for θ_l, q_w, u, and v are plotted in Figs. 3a,b (solid lines) and show a well-mixed subcloud layer up to 500 m and a conditionally unstable layer from 500 to 1200 m. For simplicity, we imposed a mixing length profile following B81b, with a constant mixing length inside the cloud layer (Fig. 4). A dynamically determined mixing length profile as used in BFP92 would be more suitable, but in the present case an accurate computation of the turbulent length scales would require the knowledge of the thermodynamic profiles in a cumulus updraft. All other details concerning the initialization and the experiment can be found in the cited references.

Two simulations were run, simulation A with a constant in-cloud mixing length of 150 m and simulation B using a value of 300 m. The vertical resolution of the model was 100 m. All the model results are shown after 3 hours of simulation. Initially, no clouds exist in the model. They form as a result of upward moisture transport into the conditionally unstable layer. In simulation B the cloud layer extends up to 1500 m (dashed lines in Figs. 3a,b) instead of 1200 m when a mixing length of 150 m is used. In Fig. 5a we compare the simulated liquid water

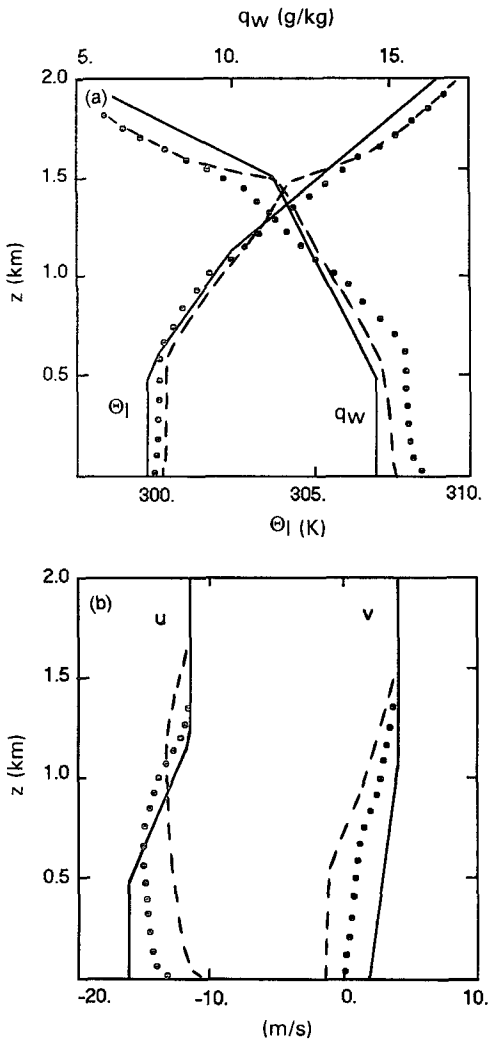

FIG. 3. Initial and modeled profiles of θ_l, q_w (a) and the horizontal wind components (b) for the Puerto Rico case. Initial profiles: solid lines; simulation A: l_K cloud = 150 m, dashed lines; simulation B: l_K cloud = 300 m, dotted lines.

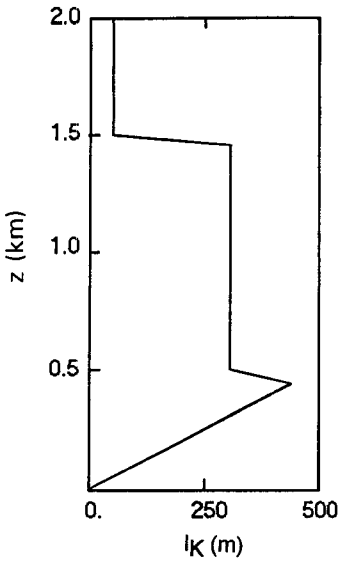

FIG. 4. Vertical profile of the mixing length for simulation B.

content to the results of S76, CD93, and B81b. The results of simulation B compare well to those obtained by B81b, but simulation A produces a cloud layer of insufficient vertical extent. However, the maximum liquid water content in the LES of S76 and CD93 is higher, with a maximum value of 0.015 g kg^{-1} compared to a value of 0.01 g kg^{-1} in simulation B.

An interesting aspect of Fig. 5a is that the LES models produce a parabolic profile of the liquid water content in contrast to a quasi-constant profile in the present model and in B81b. This difference is due to the fact that the latter models use a simple constant in-cloud mixing length. The dependence of the present simulations on the value of the mixing/dissipation length is obvious as these length scales not only affect turbulent diffusion, and so the mean profiles of θ_l and q_w, but also modify the computation of σ_s by (10), and so the computation of q_l. It is this latter effect that is the most important in this low cloudiness case, where σ_s should be known rather precisely. It is only after the formation of the first clouds that the model produces the right turbulent transport via the liquid water flux term in the buoyancy flux.

In Fig. 5b are also plotted the vertical profiles of the partial cloudiness for simulations A and B. The partial cloudiness is nearly constant with height with maximum values of about 3% for simulation A and 5% for simulation B. The corresponding profile obtained by CD93 exhibits maximum values similar to simulation B, but the cloudiness decreases with height. Finally, in Fig. 6 we compare the liquid water flux computed from (14) to the results of B81a and S76. Both models give a higher liquid water flux. The difference is due to the simplification in (14) (γ was set to 1). However, tests showed that the corresponding formulation [Eq. (18) in B81a] gives a less smooth profile and tends to overestimate the liquid water flux.

More information than from the vertical profiles can be obtained from the time series of the cloud cover (Fig. 7a) and the maximum liquid water content (Fig. 7b), as these quantities fluctuate rather strongly in time in both the LES and the present model. In Fig. 7a we have compared the modeled cloud cover, taken as the maximum of the partial cloudiness, to the LES results of CD93, which denote the maximum of the horizontally averaged cloud cover. After 3 hours of simulation time the cloud cover tends in both models to a value of roughly 6%. This value is lower than the observed value of 14% (Pennell and LeMone 1974). CD93

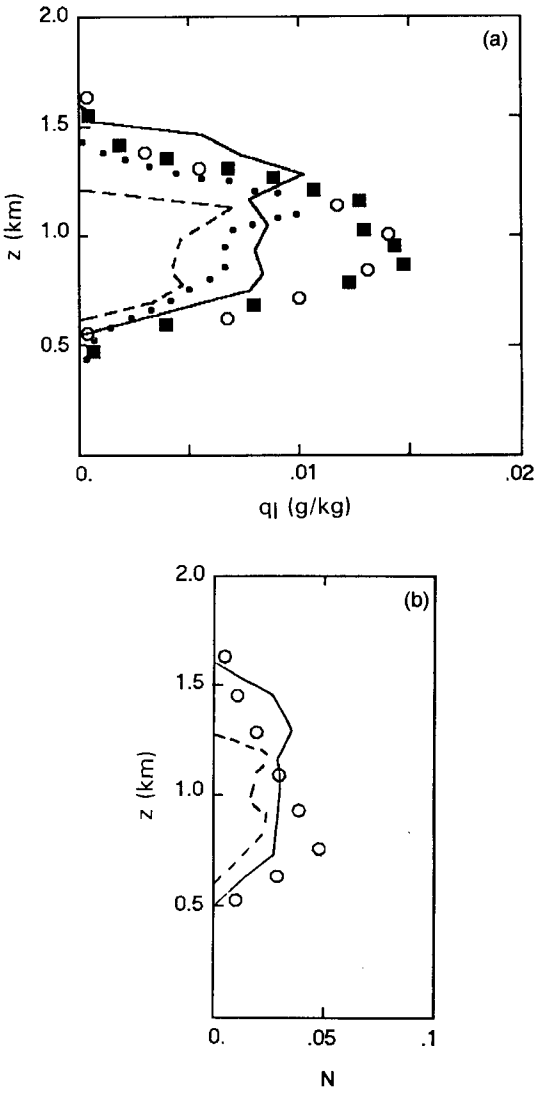

FIG. 5. (a) Simulated liquid water content. Simulation A: dashed line, simulation B: solid line, results of B81b: small full circles, LES results of S76: full squares, and LES results of CD93: open circles. (b) As in (a) but for partial cloudiness.

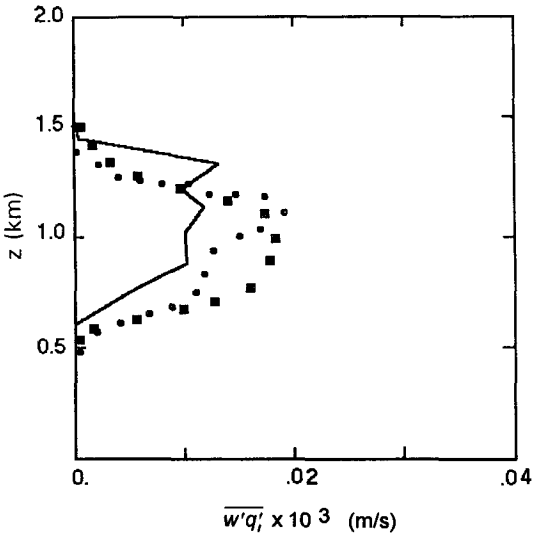

FIG. 6. Same as Fig. 5 but for the liquid water flux.

showed by vertically projecting the clouds on the surface that this difference can be explained by the strong downshear vertical extension of the clouds, an effect that is not represented by the present model. In the LES, the first clouds appear after about one hour of simulation, whereas in the present model the first clouds appear after several minutes. This difference can be explained by the fact that the cloudiness scheme in the present model is purely diagnostic. The cloud cover in simulation A slowly increases to its limit value. In simulation B, with larger mixing length, the cloud cover displays larger fluctuations but already produces after several minutes of simulation a value of the cloud cover close to its stationary value.

The time evolution of the maximum liquid water content is shown in Fig. 7b together with the results of S76, CD93, and B81b. As noted before, large variations can be found in the LES, especially in the time range between 120 and 180 min. These temporal variations depend on the size of the model domain (CD93). The results of B81b show the smoothest evolution with a final value of the maximum liquid water content of roughly 0.01 g kg^{-1}, a value also approximately obtained by the present model and the LES.

b. *Importance of the liquid water flux*

The importance of the formulation of the liquid water flux is now investigated by two additional experiments. In the first experiment we use a Gaussian function so that F_{NG} in (20) is set to 1. In the second experiment we choose $F_{NG} = Q_1^2$ so that F_{NG} is equal to the original formulation for $Q_1 = -2$, but 2.5 times larger when $Q_1 = -4$. In both experiments we compute the partial cloudiness and the cloud water content from the original expression (19). In order to get an idea of

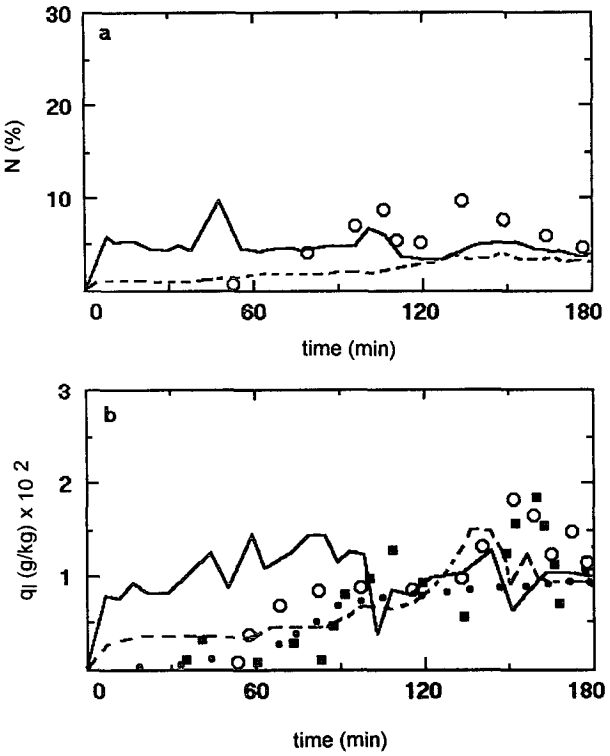

FIG. 7. Time evolution of (a) the cloud cover (taken as the maximum value of the partial cloudiness) and (b) the maximum liquid water content. Notations are the same as in Fig. 5.

the expected range of values for F_{NG}, we have plotted in Fig. 8 for the baseline experiment the vertical profile of Q_1 as well as the profile of F_{NG} obtained from (20). We see that the magnitude of Q_1 essentially varies be-

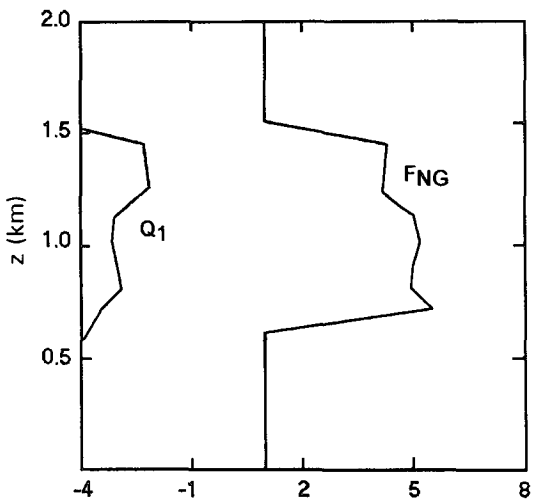

FIG. 8. Vertical profiles of Q_1 and F_{NG} corresponding to simulation B.

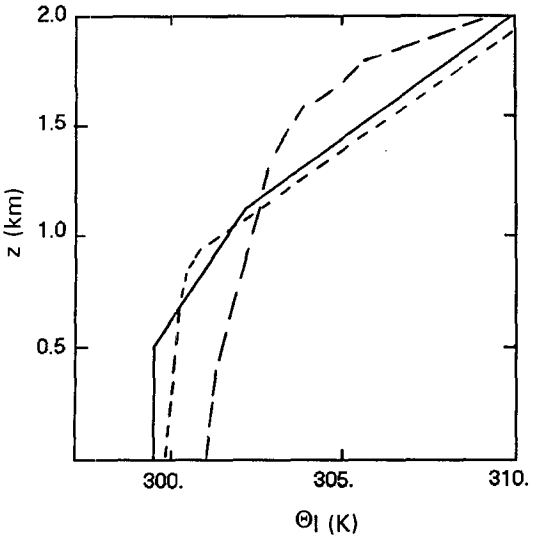

FIG. 9. Profiles of θ_l obtained with different formulations of F_{NG}. Initial profile: solid line, $F_{NG} = 1$ (Gaussian): short-dashed line, and $F_{NG} = Q_1^2$: long-dashed line.

tween 2 and 3, so that the liquid water flux is about four to five times stronger than in the Gaussian case.

The results for the two experiments mentioned above are plotted in Fig. 9 showing the corresponding vertical profiles of θ_l, as well as the initial profile. For the Gaussian distribution we get insufficient vertical transport in the conditionally stable cloud layer, resulting in a well-mixed but relatively shallow cloud layer with high cloud water content and high cloudiness of about 30% (not shown). The second experiment produced too much vertical mixing and entrainment, resulting in a thick mixed layer, where cloud formation is inhibited by too strong entrainment. This experiment therefore underlines the importance of a correct formulation of the liquid water flux in a convective situation. Therefore, the cloudiness amount in the model is much more sensitive to the formulation of the liquid water flux in the turbulence scheme than to the precise form of the distribution needed to compute N.

5. Conclusions

The aim of the present paper was to show that a low-order turbulence scheme, including a statistical subgrid-scale cloudiness scheme, can be easily extended to represent moist convection by using a positively skewed subgrid distribution function for the convective (cumulus) boundary layer, instead of the Gaussian distribution used for the stratocumulus-topped boundary layer.

A simple approach has been chosen to circumvent the problem of determining the skewness. We simply interpolate the partial cloudiness, the mean cloud water content, and the liquid water flux between two limit cases: the trade wind boundary layer characterized by a positive distribution with a skewness of 2, and the stratocumulus-topped boundary layer, which can be well represented with a Gaussian (zero skewness) function. It was shown that the main influence of the choice of the distribution function is on the liquid water flux term, which primarily determines the production of turbulent kinetic energy, the turbulent transport of heat and moisture, and finally the cloud amount.

The new scheme was incorporated in a 1D model version and tested for the case of a trade wind boundary layer observed during the Puerto Rico Field Experiment. The results compare well to those obtained with a third-order turbulence scheme and also reasonably well to those obtained with LES. This suggests that a limit distribution with a skewness of 2 seems to be quite reasonable for the trade wind boundary layer. However, it was shown that the model results depend on the turbulent mixing/dissipation length scales, two parameters that need to be known reasonably well. This is a disadvantage of the scheme against convection schemes, but these schemes have other closure problems.

This paper was devoted to present the feasibility and the potential applications of a simple unified cloudiness–turbulence scheme, and we do not claim to present a validation of such a scheme. Further work is under way to accurately determine the proportionality coefficient γ and $\overline{sq_l'}/\sigma_s^2$ in the parameterization of the liquid water flux using LES, as well as to determine the turbulent length scales in shallow convective situations.

Acknowledgments. We are especially endebted to Dr. P. Bougeault for his encouragement for this work, and to Dr. J.-P. Pinty for help on the draft. Special thanks go to the research group of KNMI, Holland (Drs. B. Holtslag, A. van Ulden, and P. Siebesma) and to P. Duynkerke (IMAU, University of Utrecht) for very stimulating discussions. This work was supported by grants from ATP PAMOS and computer resources from IDRIS (Paris) and Météo France.

APPENDIX A

Evaluation of the Distribution Integrals for the Two Proposed Models

$G(t)$	$\frac{1}{\sqrt{2\Pi}} e^{-t^2/2}$	$H(t+1)\, e^{-(t+1)}$
N	$\frac{1}{2}\left(1 + \text{erf}\frac{Q_1}{\sqrt{2}}\right)$	$Q_1 \leqslant 1 \quad e^{Q_1-1}$ $Q_1 > 1 \quad 1$
$\frac{\bar{q}_l}{\sigma_s}$	$NQ_1 + \frac{e^{-Q_1^2/2}}{\sqrt{2\Pi}}$	$Q_1 \leqslant 1 \quad e^{Q_1-1}$ $Q_1 > 1 \quad Q_1$
$\frac{\overline{sq_l'}}{\sigma_s^2}$	$\frac{1}{2}\left(1 + \text{erf}\frac{Q_1}{\sqrt{2}}\right)$	$Q_1 \leqslant 1 \quad (2 - Q_1)\, e^{Q_1-1}$ $Q_1 > 1 \quad 1$

APPENDIX B

Derivation of (17)

The buoyancy flux can be written as a sum of the liquid potential temperature flux and the total water flux:

$$F_{\theta_v} = AF_{\theta_l} + BF_{q_w}, \quad \text{(B1)}$$

where the notations are the same as in (16). The coefficients A and B possess different values for the saturated (cloudy) and unsaturated (clear sky) flux (Cuijpers and Duynkerke 1993):

for unsaturated air:

$$A = 1 + 0.61\bar{q}_w, \quad B = 0.61\bar{\theta} \quad \text{(B2.1)}$$

for saturated air:

$$A = \frac{1 - \bar{q}_w + 1.61\bar{q}_{sl}\left(1 + \dfrac{L}{R_v\bar{T}}\right)}{\left(1 + \dfrac{L}{c_p}\bar{q}_{sl,T}\right)},$$

$$B = \bar{\theta}\left(\frac{L}{c_p\bar{T}}A - 1\right) \quad \text{(B2.2)}$$

with R_v the gas constant for water vapor.

Our aim is to derive from the general formulation (13) of the buoyancy flux,

$$F_{\theta_v} = (1 + 0.61\bar{q}_w)F_{\theta_l} + \alpha F_{q_w} + \beta F_{q_l}, \quad \text{(B3)}$$

the expression for the buoyancy flux in partly cloudy layers using (B1) and (B2). From (B3) we obtain

$$F_{\theta_v} = F_{\theta_v}^{\text{clr}} + \beta F_{q_l}, \quad \text{(B4)}$$

where $F_{\theta_v}^{\text{clr}}$ is defined by (B2.1) $F_{\theta_v}^{\text{clr}} = (1 + 0.61\bar{q}_w) \times F_{\theta_l} + \alpha F_{q_w}$. Assuming that $F_{q_l} = \overline{w's}N(1 + f_{\text{NG}}) = (aF_{q_w} - bF_{\theta_l})N(1 + f_{\text{NG}})$, with f_{NG} the non-Gaussian contribution to the flux, (B4) can be further manipulated to give the final expression

$$F_{\theta_v} = (1 - N)F_{\theta_v}^{\text{clr}} + N[F_{\theta_l}(1 + 0.61\bar{q}_w) + \alpha F_{q_w}] + \beta F_{q_l} = (1 - N)F_{\theta_v}^{\text{clr}} + N[(1 + 0.61\bar{q}_w - \beta b)F_{\theta_l} + (\alpha + \beta a)F_{q_w}] + N\beta f_{\text{NG}}[aF_{q_w} - bF_{\theta_l}]. \quad \text{(B5)}$$

In order to assess the validity of (B5) we still have to verify that the second term of the rhs of (B5) is identical to the buoyancy flux for the saturated case defined by (B1) and (B2.2). The derivation is very tedious. However, it can be verified numerically that the difference between the two formulations is less than 1%.

REFERENCES

Albrecht, B. A., A. K. Betts, W. H. Schubert, and S. K. Cox, 1979: A model of the thermodynamic structure of the trade-wind boundary layer: Part I. Theoretical formulation and sensitivity tests. *J. Atmos. Sci.*, **36,** 73–89.

Ballard, S. P., B. Golding, and R. N. B. Smith, 1991: Mesoscale model experimental forecasts of the haar of northeast Scotland. *Mon. Wea. Rev.*, **119,** 2107–2123.

Bechtold, P., C. Fravalo, and J.-P. Pinty, 1992: A model of marine boundary layer cloudiness for mesoscale applications. *J. Atmos. Sci.*, **49,** 1723–1744.

——, J.-P. Pinty, and P. Mascart, 1993: The use of partial cloudiness in a warm rain parameterization: A subgrid-scale precipitation scheme. *Mon. Wea. Rev.*, **121,** 3301–3311.

Betts, A. K., 1973: Non-precipitating cumulus convection and its parameterization. *Quart. J. Roy. Meteor. Soc.*, **99,** 178–196.

Bougeault, P., 1981a: Modeling the trade-wind cumulus boundary layer. Part I: Testing the ensemble cloud relations against numerical data. *J. Atmos. Sci.*, **38,** 2414–2428.

——, 1981b: Modeling the trade-wind cumulus boundary layer. Part II: A high-order one-dimensional model. *J. Atmos. Sci.*, **38,** 2429–2439.

——, 1982: Cloud-ensemble relations based on the Gamma probability distribution for the higher-order models of the planetary boundary layer. *J. Atmos. Sci.*, **39,** 2691–2699.

Chen, J.-M., 1991: Turbulence-scale parameterization. *J. Atmos. Sci.*, **48,** 1510–1512.

Cuijpers, J. W. M., 1994: LES of cumulus convection. Ph.D. thesis, Technische Universiteit Delft, 150 pp.

——, and P. G. Duynkerke, 1993: Large eddy simulation of trade wind cumulus clouds. *J. Atmos. Sci.*, **50,** 3894–3908.

Hanson, H. P., 1981: On mixing by trade-wind cumuli. *J. Atmos. Sci.*, **38,** 1003–1014.

Krueger, S. K., 1988: Numerical simulation of tropical cumulus clouds and their interaction with the subcloud layer. *J. Atmos. Sci.*, **16,** 2221–2250.

——, and A. Bergeron, 1994: Modeling the trade cumulus boundary layer. *Atmos. Res.*, in press.

Lewellen, W. S., and S. Yoh, 1993: Binormal model of ensemble partial cloudiness. *J. Atmos. Sci.*, **50,** 1228–1237.

Mellor, G. L., 1977: The Gaussian cloud model relations. *J. Atmos. Sci.*, **34,** 356–358.

Pennell, W. T., and M. A. LeMone, 1974: An experimental study of turbulence structure in the fair weather trade-wind boundary layer. *J. Atmos. Sci.*, **31,** 1308–1323.

Pudykiewicz, R., R. Benoît, and J. Mailhot, 1992: Inclusion and verification of a predictive cloud-water scheme in a regional numerical weather prediction model. *Mon. Wea. Rev.*, **120,** 612–626.

Randall, D. A., 1987: Turbulent fluxes of liquid water and buoyancy in partly cloudy layers. *J. Atmos. Sci.*, **44,** 850–858.

——, Q. Shao, and C.-H. Moeng, 1992: A second-order bulk boundary-layer model. *J. Atmos. Sci.*, **49,** 1903–1923.

Schumann, U., and C.-H. Moeng, 1991: Plume fluxes in clear and cloudy convective boundary layer. *J. Atmos. Sci.*, **48,** 1746–1757.

Sommeria, G., 1976: Three-dimensional simulation of turbulent processes in an undisturbed trade wind boundary layer. *J. Atmos. Sci.*, **33,** 216–241.

——, and J. W. Deardorff, 1977: Subgrid-scale condensation in models of nonprecipitating clouds. *J. Atmos. Sci.*, **34,** 344–355.

Tiedtke, M., 1989: A comprehensive mass flux scheme for cumulus parameterization in large-scale models. *Mon. Wea. Rev.*, **117,** 1779–1800.